First measurement of the K⁻n → Λπ⁻ non-resonant transition amplitude below threshold

K. Piscicchia [a,b,*], S. Wycech [c], L. Fabbietti [d,e], M. Cargnelli [f], C. Curceanu [b], R. Del Grande [b,g], J. Marton [f], P. Moskal [h], A. Scordo [b], M. Silarski [h], D. Sirghi [b], M. Skurzok [h], I. Tucakovic [i], O. Vázquez Doce [d,e], J. Zmeskal [f], P. Branchini [j], E. Czerwinski [h], V. De Leo [k], E. De Lucia [b], A. Di Cicco [l,j], P. Fermani [b], S. Fiore [m,j], W. Krzemien [c], G. Mandaglio [n,o], M. Martini [b,p], E. Perez del Rio [b], A. Selce [l,j]

[a] CENTRO FERMI – Museo Storico della Fisica e Centro Studi e Ricerche "Enrico Fermi", 00184 Rome, Italy
[b] INFN, Laboratori Nazionali di Frascati, 00044 Frascati, Italy
[c] National Centre for Nuclear Research, 00681 Warsaw, Poland
[d] Excellence Cluster 'Origin and Structure of the Universe', 85748 Garching, Germany
[e] Physik Department E12, Technische Universität München, 85748 Garching, Germany
[f] Stefan-Meyer-Institut für Subatomare Physik, 1090 Wien, Austria
[g] Università degli Studi di Roma Tor Vergata, Rome, Italy
[h] Institute of Physics, Jagiellonian University, 30-348 Cracow, Poland
[i] Ruder Boskovic Institute, 10000 Zagreb, Croatia
[j] INFN Sezione di Roma Tre, Roma, Italy
[k] INFN Sezione di Roma Tor Vergata, Roma, Italy
[l] Dipartimento di Matematica e Fisica dell'Università "Roma Tre", Roma, Italy
[m] ENEA, Department of Fusion and Technology for Nuclear Safety and Security, Frascati (RM), Italy
[n] Dipartimento di Scienze Chimiche, Biologiche, Farmaceutiche ed Ambientali dell'Università di Messina, Messina, Italy
[o] INFN Sezione di Catania, Catania, Italy
[p] Dipartimento di Scienze e Tecnologie applicate, Università "Guglielmo Marconi", Roma, Italy

A R T I C L E   I N F O

A B S T R A C T

We present the analysis of K⁻ absorption processes on ⁴He leading to Λπ⁻ final states, measured with the KLOE spectrometer at the DAΦNE e^+e^- collider and extract, for the first time, the modulus of the non-resonant K⁻n → Λπ⁻ direct production amplitude about 33 MeV below the $\overline{K}N$ threshold. This analysis also allows to disentangle the K⁻ nuclear absorption at-rest from the in-flight capture, for K⁻ momenta of about 120 MeV. The data are interpreted with the help of a phenomenological model, and the modulus of the non-resonant K⁻n → Λπ⁻ amplitude for K⁻ absorption at-rest is found to be $|A_{K^- n \to \Lambda \pi^-}| = (0.334 \pm 0.018 \, \text{stat} ^{+0.034}_{-0.058} \text{syst})$ fm.

1. Introduction

Experiments with low energy negatively charged kaon beams directed on gaseous or solid targets are unique to study the antikaon–nucleon/nuclei interactions, by performing measurements of the kaonic atoms de-excitations, or by detecting the final states following K⁻ absorption processes. The capture of K⁻ mesons on light nuclear targets (He and C) at-rest was observed in old bubble chamber and emulsion experiments ([1–6]), where a high purity sample was analyzed at the price of a limited statistics. In the case of interactions at-rest the underlying mechanism consists in the capture of the strange meson in a highly excited atomic state and a successive cascade to low-lying states, followed by the K⁻ nuclear capture. Studies of kaonic atoms produced a wealth of data in the recent years [7–10] which helped to understand the kaon–nucleon/nuclei threshold processes. Besides the interactions at-rest, an important contribution from in-flight K⁻ nuclear captures was already characterized by the AMADEUS Collaboration in

previous works [11,12], using a data sample collected by the KLOE Collaboration in 2004/2005 [13]. The in-flight capture process consists in the kaon propagation through the electron cloud, followed by the nuclear absorption. Since the at-rest and in-flight interactions processes are generating different kinematic distributions in the final state, it is possible to disentangle them experimentally. Let us consider the process:

$$K^- A \rightarrow Y\pi R, \tag{1}$$

where A represents the interacting nucleus, R the residual and Y the produced hyperon (Σ or Λ). $\Sigma\pi$ pairs can be either produced in *direct formation* processes trough non-resonant absorptions of the kaon on the nucleon N, or in resonant reactions, with the intermediate formation of $\Sigma(1385)$ or $\Lambda(1405)$ states. For the $\Lambda\pi$ pair formation, besides the mentioned direct formation, also the two-step process with *internal conversion* production ($\Sigma N \rightarrow \Lambda N'$) contributes, which partially or completely fragments the original residual R. The internal conversion probability was measured to account for $\sim 50\%$ of the total $\Lambda\pi$ produced pairs in ^{4}He and ^{12}C ([1,14]), with higher rates in heavier nuclei.

The direct capture of K^- mesons on neutrons in Helium was observed in old bubble chamber experiments ([2–4]) and the momentum of the $\Lambda\pi^-$ pair in the final state, equivalent to the recoil momentum of ^{3}He, was found to exhibit two components:

- a low $\Lambda\pi^-$ momentum component which was associated [15,16] to the S-wave, isospin $I = 1$, non-resonant capture from atomic states,
- a higher $\Lambda\pi^-$ momentum component which is compatible with P-wave resonant production, but whose nature remained unclear.

According to recent calculations [17] the resonant formation is also accessible in atomic S-state K^- capture, as a result of the three body structure of the initial system ($K^- = 1$, n = 2 and ^{3}He = 3). The analysis presented in this paper aims at evaluating the distinct contributions of the resonant and non-resonant K^-n absorption on ^{4}He, in both at-rest and in-flight reactions, by studying the $\Lambda\pi$ final state. The contributions of the conversion mechanisms are taken into account to evaluate the background to the direct $\Lambda\pi$ production distributions. Accounting for the binding energy of the neutron in ^{4}He and for the recoil kinetic energy of the ^{3}He, the modulus of the non-resonant transition amplitude in the energy region of (33 ± 6) MeV below the $\overline{K}N$ threshold is measured for the K^- capture at-rest, given the known resonant ($\Sigma^{*-}(1385)$) amplitude (the uncertainty on the energy shift below the threshold is mainly determined by the width of the residual nucleus momentum distribution).

The detailed characterization of the yield and spectral shape of the non-resonant antikaon–nucleon absorption, resulting in a hyperon–pion final state below the $\overline{K}N$ threshold, is also a crucial reference to study the $\Lambda(1405)$ production in $\overline{K}$ absorption experiments. According to theoretical predictions based on the chiral unitary model [18–20] (see also the review [21]) the $\Lambda(1405)$ can be interpreted as a molecular meson–baryon state, emerging from the interference of two poles, a lower mass pole (about 1390 MeV) which is mainly coupled to the $\Sigma\pi$ channel and a high mass pole, coupled to the $\overline{K}N$ production channel, located around 1420 MeV (the next to leading order calculation of the poles masses and widths can be found in [22]). For this reason the shape of the final $(\Sigma\pi)^0$ invariant mass distribution is expected to change in function of the production channel. Moreover, the isospin interference term contributes with opposite sign to the $\Sigma^\pm\pi^\mp$ cross sections, and vanishes for $\Sigma^0\pi^0$, thus the corresponding spectral

shapes also differ. Such complex situation is well reflected by the experimental searches of the $\Lambda(1405)$ [23–27]. The $\Sigma\pi$ spectral shapes are indeed found to be very different in the position of the peak and width, depending on the initial state of the reaction and on the observed decay channel. Since the $\Lambda(1405)$ can be only observed through its strong decay in $(\Sigma\pi)^0$, the only chance to enhance the contribution of the high mass pole in the observed shape is to exploit the $\overline{K}N$ production. A detailed study of the non-resonant amplitude below the $\overline{K}N$ threshold is hence essential to achieve a precision measurement of the $\Lambda(1405)$ spectral shape.

For many spectral shapes of interest, like $\Sigma^+\pi^-$, $\Sigma^-\pi^+$ and K^-p, the scattering amplitudes are composed of both $I = 0$ and $I = 1$ states. Hence, in order to extract the properties of the resonant, $I = 0$, $\Lambda(1405)$ production experimental constrains on the $I = 1$ amplitude are also needed.

2. The KLOE detector

DAΦNE [28] is a double ring e^+e^- collider, designed to work at the center of mass energy of the ϕ particle. The ϕ meson decay produces charged kaons (with BR($K^+ K^-$) = $48.9 \pm 0.5\%$) with low momentum (~ 127 MeV/c) which are ideal to study the low energy K^--nucleus absorption processes.

The KLOE detector is characterized by a geometrical acceptance of $\sim 98\%$. It consists of a large cylindrical Drift Chamber (DC) and a fine sampling lead-scintillating fibers calorimeter [29], all immersed in an axial magnetic field of 0.52 T. The DC [30] has an inner radius of 0.25 m, an outer radius of 2 m and a length of 3.3 m. The DC entrance wall composition is 750 μm of Carbon fiber and 150 μm of Aluminum foil. The DC is filled with a mixture of Helium and Isobutane (in volume: 90% ^{4}He and 10% C_4H_{10}).

Tracks are reconstructed with a resolution of $\sigma_{\rho\phi} \sim 200$ μm in the transverse ρ–ϕ plane and of $\sigma_z \sim 2$ mm along the z-axis. The transverse momentum resolution for large polar angle tracks ($45° < \theta < 135°$) is $\sigma_{p_T}/p_T \sim 0.4\%$.

The analyzed data sample has been collected in 2004/2005 and corresponds to a total luminosity of 1.74 fb^{-1}. As will be shown in the following sections, the momenta of the Λ and π^- produced in the final state of the resonant and non-resonant processes lie in the same region of the phase space. For this reason any bias introduced by the trigger system [31] does not affect the ratio of the corresponding probabilities.

3. Particle identification

The first step of the analysis consists in the selection of a Λ candidate, which represents the signature of a K^- hadronic interaction occurred in the detector materials. The Λ candidate is reconstructed exploiting the $\Lambda \rightarrow p\pi^-$ (BR = $63.9 \pm 0.5\%$) decay. A momentum larger than 170 MeV is required for the proton in order to minimize the pion contamination to the proton track candidate sample. Details about the reconstruction of the Λ decay vertex can be found in [11,12]. The mean value of the reconstructed Λ mass, extracted from the invariant mass distribution $m_{p\pi^-}$ for the selected proton-π^- pairs, is 1115.753 ± 0.002 MeV, with a resolution of $\sigma = 0.5$ MeV, where only the statistical error is given. For the successive analysis steps, the following cut is applied on the Λ invariant mass: 1112 MeV $< m_{p\pi^-} <$ 1118 MeV, resulting in a sample of $2.2 \cdot 10^6$ events.

After the Λ reconstruction an additional π^- candidate is searched for. The K^- absorption vertex is reconstructed by extrapolating backwards the Λ path and the π^- track, applying the selection on the distance of closest approach (dca) $dca < 2$ cm. The Λ decay path, expressed as the distance between the Λ decay vertex and the K^- absorption vertex, is required to be smaller than
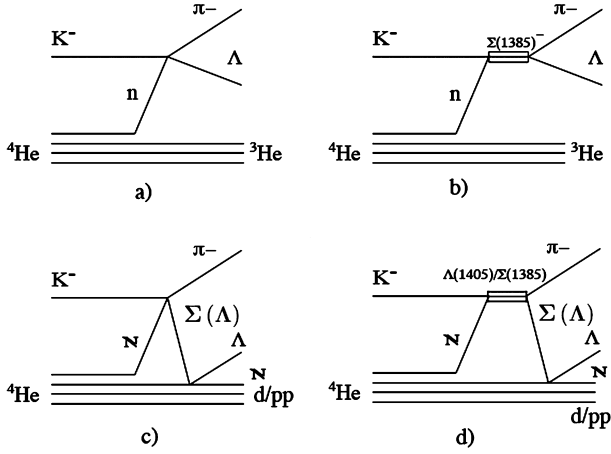
Fig. 1. Panels a) and b) show the non-resonant and resonant $\Lambda\pi^-$ direct productions, respectively. Panels c) and d) show the primary hyperon–pion formation, followed by the inelastic/elastic scattering of the Σ/Λ hyperon on a single nucleon, for the resonant and non-resonant cases, respectively. This figure was adapted from Ref. [17].

Fig. 2. (Color online.) Experimental distribution of the π^- vs Λ momenta. The red line represents the selection of the direct $\Lambda\pi^-$ production events. See the text for details.

7 cm. The radial position of the absorption vertex ($\rho_{\Lambda\pi}$) is calculated as the radial distance between the DAΦNE beam axis and the K^- absorption vertex. In order to select K^- capture events occurring in the DC gas (mainly composed of ^{4}He) the $\rho_{\Lambda\pi} > 30$ cm cut is applied. A sample of K^- absorptions on ^{12}C is also necessary in order to describe the Carbon contamination introduced by the Isobutane presence in the gas, this is obtained by selecting captures in the almost pure Carbon DC wall applying the cut $(23.8 < \rho_{\Lambda\pi} < 26.2)$ cm. The $\rho_{\Lambda\pi}$ limits are optimized on the base of Monte Carlo (MC) simulations. At this stage of the analysis a statistics of about 21500 events is selected, of $\Lambda\pi^-$ events produced following K^- absorptions in the DC gas.

4. Data analysis

All the processes contributing to the reaction:

$$K^- \, ^4\text{He} \rightarrow \Lambda\pi^- \, R, \qquad (2)$$
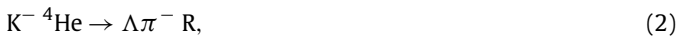
where R is the residual nucleus, are schematically represented in Fig. 1. The production of $\Lambda\pi^-$ pairs in the final state can occur either via direct non-resonant/resonant processes (a) and b) in Fig. 1) or via non-resonant/resonant two-step processes (c) and d) in Fig. 1). In the two-step processes the production of a Λ or Σ is followed by an elastic or inelastic Final State Interaction (FSI) of the hyperon. The case $\Sigma N \rightarrow \Lambda N'$ is known as the conversion process. Both the direct and the two-step processes can occur for K^- captures at-rest or in-flight.

The goal of the analysis is to extract the modulus of the non-resonant $K^- n \rightarrow \Lambda\pi^-$ transition amplitude using only the direct production processes. In Fig. 2 the measured π^- vs Λ momenta distribution is shown for K^- absorptions in the DC gas. The direct production is characterized by a strong correlation between p_Λ and p_π. The FSI of hyperons with the residual nucleons destroys this correlation. Conversion events are also shifted at lower p_π momenta as a consequence of the $\Sigma - \Lambda$ mass difference. For these reasons, the direct processes appear as rather narrow bands in Fig. 2, while the two-step processes populate an uncorrelated momentum distribution at lower values of both the pion and the lambda momenta. The red line shown in Fig. 2 represents the phase space cut used to select the direct processes, this cut was optimized based on MC simulations of direct $\Lambda\pi^-$ production, according to the calculations reported in [17]. The number of
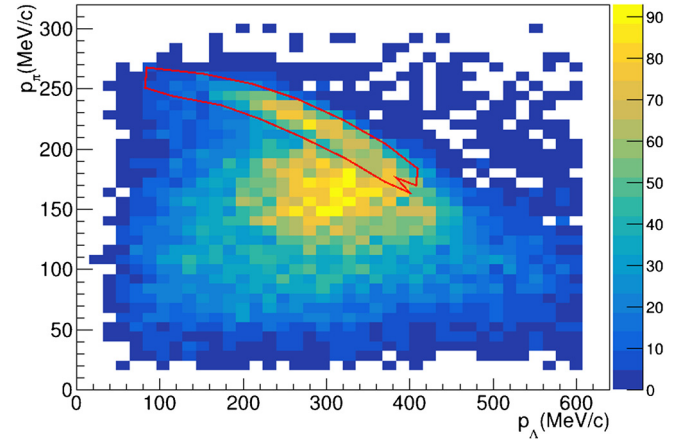
selected $\Lambda\pi^-$ events after applying this cut is 3050. Direct processes involve $K^- n \rightarrow \Lambda\pi^-$ production both at-rest (characterized by smaller π^- momenta) and in-flight (associated to higher π^- momenta). The superposition of these two components, which are highly correlated in the p_π versus p_Λ plane, generates the shape of the red contour. The phase space cut allows to suppress the background due to the production of a $\Sigma - \pi^-$ pair in the first step of the process. In this case the observed Λ particles can originate either from Σ conversions on the residual nucleons or from the decays of primary produced Σ^0s ($K^- n \rightarrow \Sigma^0\pi^-$ followed by the Σ^0 decay $\Sigma^0 \rightarrow \Lambda\gamma$). In both cases the angular correlation between $\mathbf{p}_\Lambda$ and $\mathbf{p}_\pi$ is lost and the pion momentum is lower (due to the $\Sigma - \Lambda$ mass difference). Such background events populate the region centered around $p_\Lambda \sim 320$ MeV/c and $p_\pi \sim 160$ MeV/c in Fig. 2.

Besides inelastic FSI processes, involving the conversion of the produced Σ hyperons, also elastic FSI processes can occur, namely the re-scattering of the Λ or the π^- on residual nuclear fragments. In [17] the correction to the amplitude modulus due to these contributions is found to be less than 3% of the total $K^- n \rightarrow \Lambda\pi^-$ amplitude modulus. For this reason, the elastic FSI contribution is neglected in this analysis.

Since the selected sample contains not only direct processes, but also a certain contamination from conversion processes, both are simulated and used to fit the experimental distributions, in order to extract the amplitude of direct non-resonant processes.

4.1. Direct $\Lambda\pi^-$ production simulation

Direct processes have been simulated according to a phenomenological model of the reaction $K^- \, ^4$He $\rightarrow \Lambda\pi^- \, ^3$He [17]. K^- captures both at-rest and in-flight are taken into account. In the case of absorptions at-rest S and P atomic states have been considered.

For the K^--nucleon interaction, besides the non-resonant S-wave and isospin $I = 1$ transition, also the P-wave resonant interaction is included.

The $K^- n$ interaction is estimated to occur in the region of (33 ± 6) MeV below threshold for K^- captures at-rest, which reflects a very short range interaction. Two effects contribute to the energy shift below the threshold, as shown in Ref. [17]: a) the neutron separation energy $B_n = 21$ MeV (the atomic binding energy of the negatively charged kaon can be neglected with respect to B_n), b) the recoil energy of the $K^- n$ pair with respect to the residual nucleus ^{3}He. We then have an energy shift of

$E_{\mathrm{Kn}} \sim -B_n - < \frac{p_{\Lambda\pi}^2}{2\mu_{\pi,\Lambda,3\mathrm{He}}} >$ with $\mu_{\pi,\Lambda,3\mathrm{He}}$ the appropriate reduced mass. The average recoil energy is calculated in Ref. [17] and consists of a peak with center at 12 MeV and width of 12 MeV, which represents the main uncertainty on E_{Kn}. The in-flight K^-n interaction occurs about 22 MeV below threshold due to the contribution of the kaon momentum. There seems to be no structure in the non-resonant transition amplitude, then this is assumed to be weakly energy dependent in Ref. [17] as a result of the very short range interaction.

Considering charge and isospin conservation, the only resonant contribution to the $K^{-}{}^4\mathrm{He} \rightarrow \Lambda\pi^-\,{}^3\mathrm{He}$ process is the intermediate formation of the $\Sigma^-(1385)$ resonance. Although the atomic capture happens mainly in the S-state, the $\Sigma^-(1385)$ production is allowed when the K^-n state is P-wave, since the angular momentum is conserved by a P-wave configuration between the ${}^3\mathrm{He}$ residual and the K^-n system.
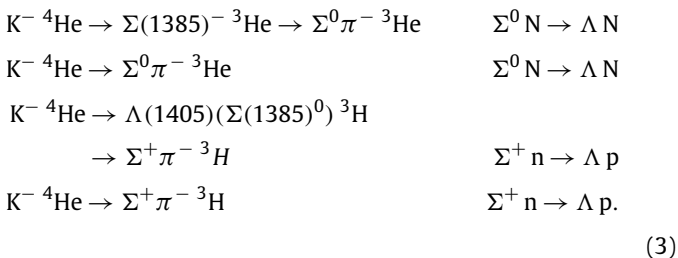
The model [17] delivers the various probability distributions for the total $\Lambda\pi$ momentum ($p_{\Lambda\pi}$). Applying energy and momentum conservation the reactions $K^{-4}\mathrm{He} \rightarrow \Lambda\pi\,{}^{-3}\mathrm{He}$ are simulated. The following notation for the input probability distributions is used:

- $P_{\mathrm{ar}}^{\mathrm{nr/res}}(p_{\Lambda\pi})$ – momentum distribution for the non-resonant and resonant production at-rest, respectively.
- $P_{\mathrm{if}}^{\mathrm{nr/res}}(\boldsymbol{p}_{\Lambda\pi}, \boldsymbol{p}_{\mathrm{K}})$ – momentum distribution for the non-resonant and resonant production in-flight, respectively.

These functions involve nuclear matrix elements, phase space elements and $K^-n \rightarrow \Lambda\pi^-$ transition amplitudes. In the non-resonant case the transition amplitude modulus $|f^{\mathrm{nr}}|$ factorizes and $P^{\mathrm{nr}} \propto |f^{\mathrm{nr}}|^2$. This quantity, denoted in many theoretical papers $|A_{K^-n\rightarrow\Lambda\pi^-}|$, is the object of our research. The kaon momentum absolute value $|\boldsymbol{p}_{\mathrm{K}}|$ is sampled according to the experimental distribution, which is obtained by selecting negatively charged kaons absorbed in the gas of the DC leading to the production of a Λ hyperon. The radial position of the absorption vertex inside the DC volume ($\rho_{\Lambda\pi}$) is sampled as well based on the experimental data, as a consequence the $\rho_{\Lambda\pi}$ distribution is not a bias for the presented analysis. For each process, the calculated $\boldsymbol{p}_\Lambda$ and $\boldsymbol{p}_\pi$ pairs are the input for the standard KLOE GEANT digitization (GEANFI [32]), followed by the event reconstruction.

4.2. $\Sigma N \rightarrow \Lambda N'$ conversion formalism

In order to account for the residual conversion background surviving the direct production phase space cut in Fig. 2, all the possible conversion processes compatible with the measured final state are simulated. The possible conversion reactions, which are listed below, are assumed to contribute with equal probabilities.

$$K^- \,{}^4\mathrm{He} \rightarrow \Sigma(1385)^- \,{}^3\mathrm{He} \rightarrow \Sigma^0\pi^- \,{}^3\mathrm{He} \qquad \Sigma^0 N \rightarrow \Lambda N$$

$$K^- \,{}^4\mathrm{He} \rightarrow \Sigma^0\pi^- \,{}^3\mathrm{He} \qquad\qquad\qquad\quad \Sigma^0 N \rightarrow \Lambda N$$

$$K^- \,{}^4\mathrm{He} \rightarrow \Lambda(1405)(\Sigma(1385)^0) \,{}^3\mathrm{H}$$

$$\qquad\qquad \rightarrow \Sigma^+\pi^- \,{}^3\mathrm{H} \qquad\qquad\qquad \Sigma^+ n \rightarrow \Lambda p$$

$$K^- \,{}^4\mathrm{He} \rightarrow \Sigma^+\pi^- \,{}^3\mathrm{H} \qquad\qquad\qquad\;\; \Sigma^+ n \rightarrow \Lambda p.$$

$$(3)$$

The first step of the processes listed in Eqs. (3), leading to $\Sigma\pi$ pair production is calculated according to [17]. The model delivers the momentum distribution of the $\Sigma\pi$ pair, by applying momentum and energy conservation, the momenta $\boldsymbol{p}_\Sigma$, $\boldsymbol{p}_\pi$ and $\boldsymbol{p}_{3\mathrm{He}/3\mathrm{H}}$ are obtained for each event. In the case of resonant production the

parameters of the involved resonances are taken from [33]. In the second step the Σ/Λ conversion occurs ($\Sigma N \rightarrow \Lambda N'$).

The momentum of the Λ in the final state was obtained with a calculation similar to the case of K^--nucleon in-flight absorption, as described in [17].

The nucleon wave function is sampled according to the Fermi distribution within the residual nucleus obtained from the first step of the calculation. A possible energy dependence of the conversion transition amplitude is neglected. For each event, the primary $\boldsymbol{p}_\pi$ and the momentum of the Λ emerging from the conversion process are the input for the standard GEANFI simulation, followed by the event reconstruction.

The outcome of the simulation is used to fit the experimental distributions and to extract the yields of the contributing processes.

4.3. K^- absorptions on ${}^{12}C$

Since the DC is filled with a mixture of Helium and Isobutane (in volume: 90% ${}^4\mathrm{He}$ and 10% C_4H_{10}), the data contain a sizeable contribution due to K^- interactions on Carbon atoms. The ratio of the reactions on Helium and on Carbon, in the DC gas, leading to a $\Lambda\pi^-$ final state has been evaluated as:

$$\frac{N_{K^{-4}\mathrm{He}}}{N_{K^{-12}\mathrm{C}}} = \frac{n_{4\mathrm{He}}\,\sigma_{K^{-4}\mathrm{He}}\,\mathrm{BR}_{K^{-4}\mathrm{He}}(\Lambda\pi^-)}{n_{12\mathrm{C}}\,\sigma_{K^{-12}\mathrm{C}}\,\mathrm{BR}_{K^{-12}\mathrm{C}}(\Lambda\pi^-)}. \qquad (4)$$

$n_{4\mathrm{He}}/n_{12\mathrm{C}}$ is the ratio of the Helium and Carbon atoms in the DC and was calculated to be about 2.26. $\sigma_{K^{-4}\mathrm{He}}$ and $\sigma_{K^{-12}\mathrm{C}}$ are the total inelastic cross sections for K^- scattering on the two nuclei, $\mathrm{BR}_{K^{-4}\mathrm{He}}(\Lambda\pi^-)$ and $\mathrm{BR}_{K^{-12}\mathrm{C}}(\Lambda\pi^-)$ are the branching ratios for the $\Lambda\pi^-$ production following K^- absorption in Helium and Carbon, respectively. Experimental low energy cross sections on Helium and Carbon for K^- momentum ~ 100 MeV/c are not available, the ratio $\sigma_{K^{-4}\mathrm{He}}/\sigma_{K^{-12}\mathrm{C}} = 0.4$ was then obtained from the values calculated in [34,35]. The ratio $\mathrm{BR}_{K^{-4}\mathrm{He}}(\Lambda\pi^-)/\mathrm{BR}_{K^{-12}\mathrm{C}}(\Lambda\pi^-)$ was set to 1.4 ± 0.4 according to [14].

The value obtained for the Helium to Carbon ratio is:

$$\frac{N_{K^{-4}\mathrm{He}}}{N_{K^{-12}\mathrm{C}}} = 1.27 \pm 0.3. \qquad (5)$$

The error accounts only for the branching ratio uncertainty. This translates into a probability of $(44 \pm 13)\%$ for the measured $\Lambda\pi^-$ final state to be originated from a K^- absorption on Carbon.

In order to consider this contribution in the interpretation of the measured $\Lambda\pi^-$ final state, an experimental sample containing $K^-\,{}^{12}\mathrm{C}$ interactions is used. This sample was obtained by selecting kaons which interact in the DC entrance wall ($\rho_{\Lambda\pi} = 25 \pm 1.2$ cm). MC simulations show that the π^- and Λ momentum resolutions obtained for this sample are comparable to the resolutions in gas since the DC wall is rather thin. The Carbon-sample is selected using the same criteria as for the gas sample and was used in the global fit. In order to take the error introduced by the selection of $\rho_{\Lambda\pi}$ into account, it is varied such as to increase and decrease the number of $\Lambda\pi^-$ candidate events by 15%. This variation is considered as a systematic error of the kinematic distributions corresponding to K^- absorption on Carbon.

4.4. Results

In order to extract the ratio of the resonant over non-resonant $\Lambda\pi^-$ production, the measured $p_{\Lambda\pi}$, $m_{\Lambda\pi}$ (invariant mass of the hyperon–pion pair) and $\cos(\theta_{\Lambda\pi})$ ($\theta_{\Lambda\pi}$ is the angle between the Λ and π momenta) distributions were fitted. The simulated distributions of the direct $\Lambda\pi^-$ production in ${}^4\mathrm{He}$ and the background
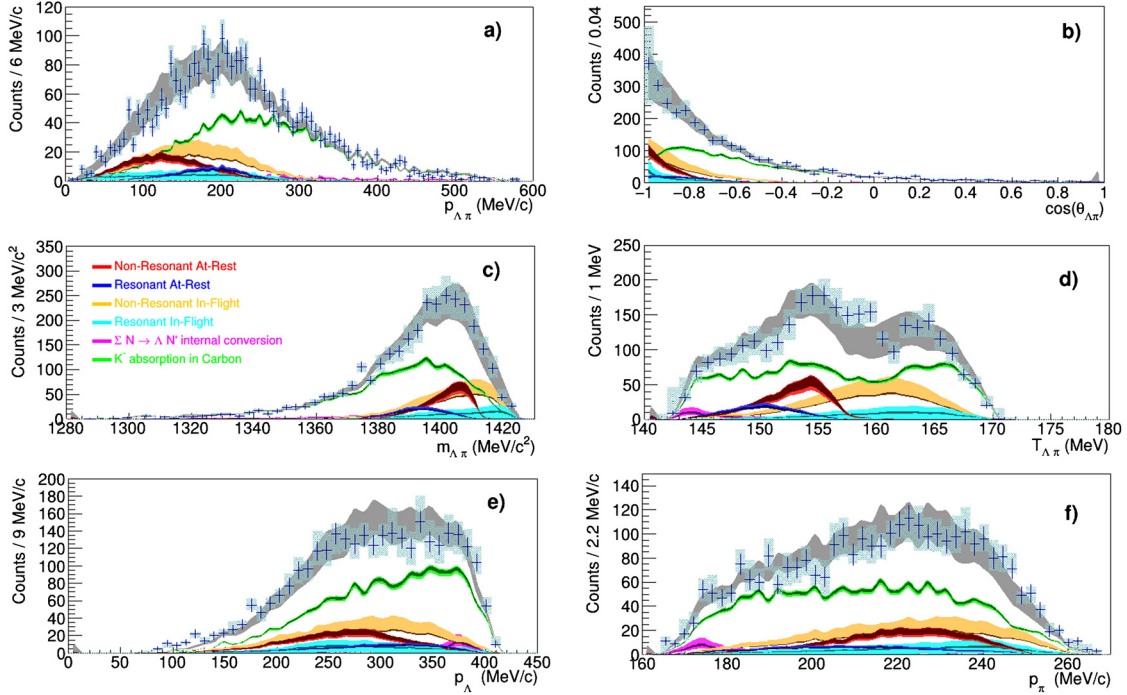
Fig. 3. (Color online.) Panels a)–f): $p_{\Lambda\pi}$, $\cos(\theta_{\Lambda\pi})$, $m_{\Lambda\pi}$, $T_{\Lambda\pi}$, p_{Λ} and p_{π} distributions. The experimental data and the corresponding statistical errors are represented by the blue crosses, the systematic errors are light blue boxes. The different contributions included in the fit are shown by the colored histograms: non-resonant at-rest (red), resonant at-rest (blue), non-resonant in-flight (brown), resonant in-flight (cyan), $\Sigma N \rightarrow \Lambda N'$ internal conversion (magenta), K^- absorptions in Carbon (green). The light and dark bands correspond to systematic and statistical errors, respectively. The gray band shows the total fit with the corresponding statistical error. See text for details.

components corresponding to the $\Sigma N \rightarrow \Lambda N'$ conversion process, as well as the contamination due to K^- captures on Carbon, are used in the fit to the experimental data.

The $p_{\Lambda\pi}$, $m_{\Lambda\pi}$ and $\cos(\theta_{\Lambda\pi})$ measured spectra are fitted simultaneously with the following contributions:

- non-resonant K^- capture at-rest from atomic S states in ^{4}He,
- resonant K^- capture at-rest from atomic S states in ^{4}He,
- non-resonant K^- capture in-flight in ^{4}He,
- resonant K^- capture in-flight in ^{4}He,
- primary $\Sigma\pi^-$ production followed by the $\Sigma N \rightarrow \Lambda N'$ conversion process,
- K^- capture processes in ^{12}C giving rise to $\Lambda\pi^-$ in the final state.

The contribution of the K^- captures at-rest from atomic P states are found to be negligibly small. Also in the results reported by the KEK and SIDDHARTA Collaborations ([36,37]) it is shown that due to molecular collisions K^- captures mainly occur from high n,S states of the atom.

The modulus of the amplitude of the non-resonant processes, the ratio of the resonant to non-resonant processes, the modulus of the amplitude of the conversions and the contribution of the K^- captures on Carbon are considered as free parameters in the fit.

Panels a)–f) in Fig. 3 show $p_{\Lambda\pi}$, $\cos(\theta_{\Lambda\pi})$, $m_{\Lambda\pi}$ distributions used for the fit and, additionally, the total hyperon–pion kinetic energy $T_{\Lambda\pi}$, as well as the moduli of the p_{Λ} and p_{π} momenta. The systematic errors are estimated by varying independently the selection of the radial position of the K^- absorption point $\rho_{\Lambda\pi}$ inside the DC and the geometrical cut in the p_{π}–p_{Λ} scatter plot that selects the direct $\Lambda\pi^-$ production region, such as to increase or decrease the $\Lambda\pi^-$ statistics by 15% with respect to the optimized selection. In order to take into account the error introduced by the DC entrance wall selection ($\rho_{\Lambda\pi} = 25 \pm 1.2$ cm), this cut

Table 1
Resonant to non-resonant ratios and amplitudes of the various channels extracted from the fit of the $\Lambda\pi^-$ sample. The statistical and systematic errors are also shown. See text for details.

Channels	Ratio/yield	σ_{stat}	σ_{syst}
RES-ar/NR-ar	0.39	± 0.04	$^{+0.18}_{-0.07}$
RES-if/NR-if	0.23	± 0.03	$^{+0.23}_{-0.22}$
NR-ar	12.0%	$\pm 1.7\%$	$^{+2.0}_{-2.8}\%$
NR-if	19.2%	$\pm 4.4\%$	$^{+5.9}_{-3.3}\%$
$\Sigma \rightarrow \Lambda$ conv.	2.2%	$\pm 0.3\%$	$^{+1.6}_{-0.8}\%$
$K^- {}^{12}$C capture	57.0%	$\pm 1.2\%$	$^{+2.2}_{-3.2}\%$

is also varied independently such as to increase and decrease the number of $\Lambda\pi^-$ vertices in the Carbon wall by 15%.

The systematic errors of the fit were evaluated as follows. First the fit is carried out by setting the contribution of the $K^- {}^{12}$C captures to the value estimated in the previous Section. The systematic error is evaluated by repeating the fit letting the $K^- {}^{12}$C captures contribution free. The free Carbon fit requires an increased contribution from $K^- {}^{12}$C captures as big as 61.4%. Half of the difference between the result of the free fit (61.4%) and the maximum expected background (57%) is considered for the Carbon sample to estimate the final systematic errors for all the fit components.

The chi-square of the fit is $\chi^2/ndf = 151/148$. Table 1 shows the fit results, where the resonant to non-resonant ratios for at-rest and in-flight reactions are shown together with the yields of the various channels obtained from the fit.

The ratio of the resonant over non-resonant $\Lambda\pi^-$ production in-flight is found to be smaller than the corresponding ratio at-rest. This is not surprising as the K^-n interaction in-flight occurs about 20 MeV below the $\overline{K}N$ threshold; the corresponding reaction at-rest occurs about 33 MeV below the threshold, nearer to the resonance which lays about 49 MeV below the $\overline{K}N$ threshold.

Table 2
The S-wave non-resonant amplitude ($|f^{nr}|$ fm) extracted from $K^-p \to \Lambda\pi^0$ scattering [38,39] and from this experiment ($E = -33$ MeV).

$E = -33$ MeV	$0.334 \pm 0.018\, \text{stat}^{+0.034}_{-0.058}\, \text{syst}$
$p_{lab} = 120$ MeV	0.33 ± 0.11
$p_{lab} = 160$ MeV	0.29 ± 0.10
$p_{lab} = 200$ MeV	0.24 ± 0.06
$p_{lab} = 245$ MeV	0.28 ± 0.02

The systematic uncertainty on the resonant to non-resonant ratio for the in-flight reactions, prevents from extracting the modulus of the non-resonant transition amplitude in-flight.

The $\Lambda\pi^-$ momentum distributions ($P_{ar}^{nr/res}(p_{\Lambda\pi})$) for the K^-n non-resonant and resonant absorption at-rest, introduced in Section 4.1, are given in Eq. (14) and Eq. (20) of Ref. [17], respectively. The modulus of the non-resonant $K^-n \to \Lambda\pi^-$ transition amplitude ($|f_{ar}^{nr}|$) involved in $P_{ar}^{nr/res}(p_{\Lambda\pi})$ is assumed to be constant. To obtain its value we calculate the ratio ($\frac{NR-ar}{RES-ar}$) between the measured number of $\Lambda\pi^-$ pairs produced in non-resonant (NR) and resonant (RES) K^- absorptions in ^{4}He at-rest (ar). This ratio is then equated to the ratio of the integrals of the corresponding momentum distributions $P_{ar}^{nr/res}(p_{\Lambda\pi})$, which leads to:

$$\frac{NR-ar}{RES-ar} = \frac{\int_0^{pmax} P_{ar}^{nr}(p_{\Lambda\pi})\,dp_{\Lambda\pi}}{\int_0^{pmax} P_{ar}^{res}(p_{\Lambda\pi})\,dp_{\Lambda\pi}} =$$
$$= |f_{ar}^{nr}|^2 \cdot 8.94 \cdot 10^5 \text{ MeV}^2. \qquad (6)$$

Once the constant $|f_{ar}^{nr}|^2$ is factorized in the numerator the ratio of the remaining integrals gives the numerical factor which results from the integrals presented in Ref. [17]. The ratio $\frac{NR-ar}{RES-ar}$ determined by the experiment then yields:

$$|f_{ar}^{nr}| = |A_{K^-n \to \Lambda\pi^-}| = (0.334 \pm 0.018\, \text{stat}^{+0.034}_{-0.058}\, \text{syst})\, \text{fm}. \qquad (7)$$

5. Discussion

In this work the direct $\Lambda\pi^-$ production events from low energy K^-n captures in ^{4}He were identified and the contributions from K^- absorptions at-rest and in-flight ($p_K \sim 100$ MeV) were disentangled. The measured $p_{\Lambda\pi}$, $m_{\Lambda\pi}$ and $\cos(\theta_{\Lambda\pi})$ spectra were fitted with calculated distributions expressed in terms of $K^-n \to \Lambda\pi^-$ transition amplitudes: the isospin $I = 1$ S-wave amplitude and the resonant $I = 1$ P-wave amplitude which is dominated by the $\Sigma^-(1385)$. The resonant amplitude is well known from direct experiments and was used to extract the non-resonant $|A_{K^-n \to \Lambda\pi^-}|$ for atomic captures for the first time.

The $|A_{K^-n \to \Lambda\pi^-}|$ extracted using this method describes the $K^-n \to \Lambda\pi^-$ transition at about 33 MeV below the K^-n threshold, according to the energy shift obtained in Ref. [17]. Thus it allows an extrapolation to the un-physical region and should be used to test models of S-wave interaction. Such extrapolation is also of interest in the studies of the $\Lambda(1405)$ as it helps to determine the background $I = 1$ amplitude. One can compare the sub-threshold result with the corresponding values extracted from $K^-p \to \Lambda\pi^0$ cross sections [38,39] shown in Table 2. The sub-threshold S-wave amplitude is compatible with the above threshold measurements and seems to remain rather constant over the considered energy range.

In Ref. [40] and Ref. [41] the real and imaginary parts of the non-resonant coupled channels $K^-n \to \Lambda\pi / \Sigma\pi$ scattering amplitudes, calculated on the basis of several chiral SU(3) meson–baryon coupled channels interaction models (Prague (P) [42], Kyoto–Munich (KM) [22], Murcia (M1, M2) [43] Bonn (B2, B4) [44]) are
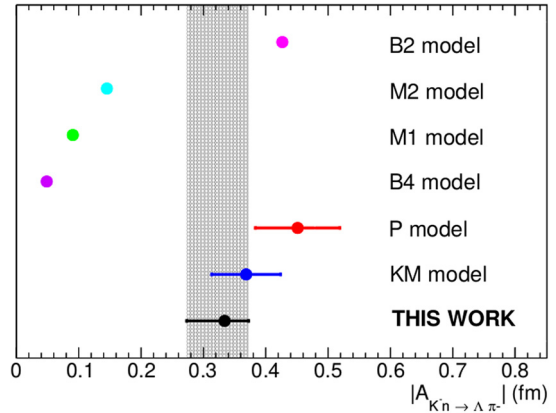

Fig. 4. (Color online.) Modulus of the measured non resonant $K^-n \to \Lambda\pi^-$ transition amplitude compared with theoretical calculations, see details in the text.

shown. Since the $K^-n \to \Sigma\pi$ non-resonant amplitude modulus was not measured, the comparison of the theoretical results with the present measurement requires the extraction of the theoretically predicted $|A_{K^-n \to \Lambda\pi^-}|$ value (for the $\Lambda\pi^-$ final state) from the real and imaginary parts of the total K^-n non-resonant absorption scattering amplitude modulus ($|A_{K^-n}|$) presented in Ref. [40] and Ref. [41]. This was performed as follows:

- for each model the amplitude modulus $|A_{K^-n}|$ is calculated in the energy region of 33 ± 6 MeV below the $\overline{K}N$ threshold, according to the estimate described in Section 4.1. It is to be stressed that the value of the in-medium energy of the two body $\overline{K}N$ subsystem slightly differs, depending on the adopted prescription (see for example references [45–47]). Nevertheless, the comparison of the measured transition amplitude with the theoretical predictions is weakly dependent on the precise value of such energy shift, given that the models predictions are quite constant in the energy range (1390 ÷ 1432) MeV, except for M2. Moreover M2 is not compatible with the experimental value for all the theoretically predicted energy shifts.

- $|A_{K^-n \to \Lambda\pi^-}|$ is extracted from the total amplitude modulus $|A_{K^-n}|$ by calculating the ratios between the probabilities of the $K^-n \to \Lambda\pi^-$ and $K^-n \to \Sigma^{-/0}\pi^{0/-}$ processes, which are allowed by the electric charge conservation. Such ratios are given by:

$$\frac{Prob_{K^-n \to \Lambda\pi^-}}{Prob_{K^-n \to \Sigma^-\pi^0}} = \frac{Ph_{K^-n \to \Lambda\pi^-}}{c_1 Ph_{K^-n \to \Sigma^-\pi^0}} \qquad (8)$$

$$\frac{Prob_{K^-n \to \Lambda\pi^-}}{Prob_{K^-n \to \Sigma^0\pi^-}} = \frac{Ph_{K^-n \to \Lambda\pi^-}}{c_2 Ph_{K^-n \to \Sigma^0\pi^-}} \qquad (9)$$

where we indicated with $c_{1,2}$ the Clebsch–Gordan coefficients of the isospin $I = 1$ components of the $\Sigma^{-/0}\pi^{0/-}$ states and with $Ph_{K^-n \to Y\pi}$ the phase space factor of the generic $K^-n \to Y\pi$ process.

The obtained rescaled amplitudes are shown in Fig. 4, together with the result of this analysis, with combined statistical and systematic errors. For the KM and P models a theoretical uncertainty of 15% is quoted; for the other models the uncertainty is not available. The method described in this work gives the first experimental determination of the modulus of the non-resonant transition amplitude $|A_{K^-n \to \Lambda\pi^-}|$ below threshold, consistent with the formalism presented in Ref. [17], with a precision comparable to that obtained from scattering experiments and, hence, can be used to test S-wave interaction models.

Acknowledgements

References

[1] P.A. Katz, et al., Phys. Rev. D 1 (1970) 1267.
[2] K. Brunnel, et al., Phys. Rev. D 2 (1970) 98.
[3] D. Riley, et al., Phys. Rev. D 11 (1975) 3065.
[4] Proceedings of the International Conference on Hypernuclear Physics held at Argonne National Laboratory, May 5–7, 1969.
[5] P.J. Carlson, et al., Nucl. Phys. 74 (1965) 642.
[6] A. Barbaro-Galtieri, et al., Phys. Lett. A 5 (1963) 63.
[7] M. Bazzi, et al., Phys. Lett. B 704 (2011) 113.
[8] M. Bazzi, et al., Phys. Lett. B 714 (2012) 40.
[9] M. Bazzi, et al., Nucl. Phys. A 907 (2013) 69.
[10] M. Bazzi, et al., Nucl. Phys. A 954 (2016) 7.
[11] C. Curceanu, et al., Acta Phys. Pol. B 46 (2015) 203.
[12] O. Vazquez Doce, et al., Phys. Lett. B 758 (2016) 134.
[13] F. Bossi, E. De Lucia, J. Lee-Franzini, S. Miscetti, M. Palutan, KLOE Collaboration, Riv. Nuovo Cimento 31 (2008) 531.
[14] C. Vander Velde-Wilquet, et al., Nuovo Cimento A 39 (1977) 538.
[15] J. Uretsky, et al., Phys. Rev. D 2 (1970) 119.
[16] B.R. Wienke, Phys. Rev. D 1 (1970) 2514.
[17] K. Piscicchia, S. Wycech, C. Curceanu, Nucl. Phys. A 954 (2016) 75.
[18] J.A. Oller, U.G. Meissner, Phys. Lett. B 500 (2001) 263.
[19] T. Hyodo, et al., Phys. Rev. C 68 (2003) 018201.
[20] D. Jido, et al., Nucl. Phys. A 725 (2003) 181.
[21] T. Hyodo, D. Jido, Nucl. Phys. 67 (2012) 55.
[22] Y. Ikeda, T. Hyodo, W. Weise, Nucl. Phys. A 881 (2012) 98.
[23] D.W. Thomas, et al., Nucl. Phys. B 56 (1973) 15.
[24] R.J. Hemingway, et al., Nucl. Phys. B 253 (1985) 742.
[25] I. Zychor, et al., Phys. Lett. B 660 (2008) 167.
[26] K. Moriya, et al., Phys. Rev. C 87 (2013) 035206.
[27] G. Agakishiev, et al., HADES Collaboration, Phys. Rev. C 87 (2013) 025201.
[28] A. Gallo, et al., Conf. Proc. C 060626 (2006) 604.
[29] M. Adinolfi, et al., Nucl. Instrum. Methods A 482 (2002) 364.
[30] M. Adinolfi, et al., Nucl. Instrum. Methods A 488 (2002) 51.
[31] M. Adinolfi, et al., Nucl. Instrum. Methods A 492 (2002) 134.
[32] F. Ambrosino, et al., Nucl. Instrum. Methods A 534 (2004) 403.
[33] K.A. Olive, et al., Particle Data Group, Chin. Phys. C 38 (2014) 090001.
[34] A. Deloff, J. Law, Phys. Rev. C 10 (1974) 1688.
[35] C. García-Recio, A.J. Melgarejo, J. Nieves, Phys. Rev. C 67 (2003) 047601.
[36] S. Okada, et al., Phys. Lett. B 653 (2007) 387.
[37] M. Bazzi, et al., Phys. Lett. B 681 (2009) 310.
[38] J.K. Kim, Columbia University Report, 1966, Nevis 149.
[39] J.K. Kim, Phys. Rev. Lett. 19 (1977) 1074.
[40] J. Hrtankova, J. Mares, Phys. Rev. C 96 (2017) 015205.
[41] A. Cieplý, et al., Nucl. Phys. A 954 (2016) 17.
[42] A. Cieplý, J. Smejkal, Nucl. Phys. A 881 (2012) 115.
[43] Z.H. Guo, J.A. Oller, Phys. Rev. C 87 (2013) 035202.
[44] M. Mai, U.G. Meißner, Nucl. Phys. A 900 (2013) 51.
[45] A. Cieplý, et al., Phys. Lett. B 702 (2011) 402.
[46] T. Hoshino, et al., Phys. Rev. C 96 (2017) 045204.
[47] N. Barnea, E. Friedman, A. Gal, Nucl. Phys. A 968 (2017) 35.